Analytical Biochemistry 466 (2014) 51–58

Contents lists available at ScienceDirect

Analytical Biochemistry

journal homepage: www.elsevier.com/locate/yabio

Electrochemical biosensor based on functional composite nanofibers for detection of K-ras gene via multiple signal amplification strategy

Xiaoying Wang [a,*], Guofang Shu [b], Chanchan Gao [c], Yu Yang [a], Qian Xu [a], Meng Tang [a]

[a] Key Laboratory of Environmental Medicine and Engineering, Ministry of Education, School of Public Health, Southeast University, Nanjing 210009, China
[b] Department of Clinical Laboratory Medicine, Zhongda Hospital, Southeast University, Nanjing 210009, China
[c] Department of Oncology, Zhongda Hospital, Southeast University, Nanjing 210009, China

ARTICLE INFO

Article history:
Received 3 June 2014
Received in revised form 10 August 2014
Accepted 20 August 2014
Available online 28 August 2014

Keywords:
Functional composite nanofibers
Electrospinning
K-ras gene
Sandwich format
Signal amplification

ABSTRACT

An electrochemical biosensor based on functional composite nanofibers for hybridization detection of specific K-ras gene that is highly associated with colorectal cancer via multiple signal amplification strategy has been developed. The carboxylated multiwalled carbon nanotubes (MWCNTs) doped nylon 6 (PA6) composite nanofibers (MWCNTs–PA6) was prepared using electrospinning, which served as the nanosized backbone for thionine (TH) electropolymerization. The functional composite nanofibers [MWCNTs–PA6–PTH, where PTH is poly(thionine)] used as supporting scaffolds for single-stranded DNA1 (ssDNA1) immobilization can dramatically increase the amount of DNA attachment and the hybridization sensitivity. Through the hybridization reaction, a sandwich format of ssDNA1/K-ras gene/gold nanoparticle-labeled ssDNA2 (AuNPs–ssDNA2) was fabricated, and the AuNPs offered excellent electrochemical signal transduction. The signal amplification was further implemented by forming network-like thiocyanuric acid/gold nanoparticles (TA/AuNPs). A significant sensitivity enhancement was obtained; the detection limit was down to 30 fM, and the discriminations were up to 54.3 and 51.9% between the K-ras gene and the one-base mismatched sequences including G/C and A/T mismatched bases, respectively. The amenability of this method to the analyses of K-ras gene from the SW480 colorectal cancer cell lysates was demonstrated. The results are basically consistent with those of the K-ras Kit (HRM: high-resolution melt). The method holds promise for the diagnosis and management of cancer.

The ras gene, a proto oncogene, contains four exon sequences, distributes in the total length of approximately 30 kb DNA, and encodes a (mostly) nuclear phosphoprotein of 21 kDa [1,2]. H-, N-, and K-ras are the main members of the ras family. Ras family members normally cycle between active GTP-bound and inactive GDP-bound states, and they function at cellular membranes to transmit signals originating from extracellular stimuli to influence cell growth, proliferation, differentiation, and survival [3]. Oncogenic missense mutations at codons 12, 13, 61, and 146 strongly attenuate GTPase activity and cause ras to accumulate in the GTP-bound state, resulting in formation and progression of the cancer [4]. K-ras is the most frequently mutated ras isoform, with an incidence of approximately 15% across all human tumor types [5,6]. K-ras mutations have also been associated with increased tumorigenicity and poor prognosis [7,8]. Therefore, specific recognition and quantitative detection of K-ras and the mutations in K-ras are extremely crucial in fundamental research and clinical practice.

Up to now, a variety of methods for measuring K-ras mutation have been reported. The conventional electrophoresis-based methods, such as restriction fragment length polymorphism [9,10], denaturing gradient gel electrophoresis [11], and single-strand conformation polymorphism [12], are complicated and time-consuming. Furthermore, hazardous materials, including radioactive isotopes and ethidium bromide, were used. Direct sequencing [13,14] is expensive and not sensitive enough to detect low-abundant mutations. Real-time quantitative polymerase chain reaction (RQ–PCR)[1] [15,16] has the advantage of higher analytical

* Corresponding author. Fax: +86 25 83272561.
E-mail address: wxy@seu.edu.cn (X. Wang).

[1] *Abbreviations used:* RQ–PCR, real-time quantitative polymerase chain reaction; MWCNT, multiwalled carbon nanotube; PA6, nylon 6; Py, pyrrole; ssDNA, single-stranded DNA; wtp53, wild-type p53; mtp53, muted-type p53; TH, thionine; PTH, poly(thionine); AuNP, gold nanoparticle; TA, thiocyanuric acid; FESEM. field-emission scanning electron microscopy; DPV, differential pulse voltammetry; CV, cyclic voltammetry; GC, glassy carbon; PBS, phosphate-buffered saline; dsDNA, double-stranded DNA; 3D, three-dimensional.

http://dx.doi.org/10.1016/j.ab.2014.08.023
0003-2697/

sensitivity for mutation detection. However, the use of organic dye-labeled oligonucleotide probes makes its cost high. Compared with direct sequencing and RQ–PCR methods, SNaPshot assay [17,18] can simultaneously screen several mutations and reduce the cost of assays. Nevertheless, this method still requires expensive instruments and technical expertise. Recently, the DNA-based biosensor for the detection of K-ras mutations has generated considerable interest for simple, rapid, and inexpensive testing of genetic and infectious diseases. The sensors can translate the genetic recognition event into a corresponding analytical signal through electrochemical [19–21], optical [22–24], and electrochemiluminescence [25,26] methods. Among them, electrochemical DNA biosensors rely on the immobilization of a single-stranded oligonucleotide probe onto an electrochemical transducer surface to recognize its complementary target sequence. The high sensitivity of such devices, coupled with their high compatibility, portability, low cost, and minimal power requirements, makes them excellent candidates for DNA diagnostics [19–21].

Various nanomaterials have been used as electrochemical transducer surface to immobilize the oligonucleotide probe in electrochemical DNA biosensors during the past decade [27]. It is still a big challenge to make the biological recognition molecule utmost and stability immobilizing on the supporting scaffolds [28]. The nanofibers produced by electrospinning processes have advantages of uniformity, porosity, mechanical strength, and large surface areas [29,30]. It is believed that electrospun nanofibers can be used as an ideal platform for highly sensitive biosensing applications with the characteristics of high surface area for loading, capability of functional immobilization with desired spacing, reproducibility, and long-term storage [31]. Several reports have investigated the development of nanofiber-based biosensing platforms for biomolecular detection such as glucose [32] and protein [33]. But a biosensor based on electrospun nanofibers has never been studied to detect the ras gene.

Recently, we developed a novel electrochemical biosensor based on functional composite nanofibers for sensitive hybridization detection of p53 tumor suppressor using methylene blue as an electrochemical indicator [34]. In the strategy, carboxylated multiwalled carbon nanotubes (MWCNTs) doped nylon 6 (PA6) composite nanofibers (MWCNTs–PA6) were prepared using electrospinning, which served as the nanosized backbone for pyrrole (Py) electropolymerization. The functional composite nanofibers (MWCNTs–PA6–PPy) used as supporting scaffolds for single-stranded DNA (ssDNA) immobilization can increase the amount of DNA attachment. The biosensor displays good sensitivity, good specificity, and a high degree of discrimination between the wild-type p53 sequence (wtp53) and the muted-type p53 sequence (mtp53). To improve the detection sensitivity significantly, remarkable adjustments have been made to the sensing system. Here, an electrochemical biosensor based on functional composite nanofibers for hybridization detection of specific K-ras gene, which is highly associated with colorectal cancer via the multiple signal amplification strategy, is developed. The electrospun nanofibers (MWCNTs–PA6) served as the nanosized backbone for thionine (TH) electropolymerization via two steps (see Materials and Methods). The functional composite nanofibers [MWCNTs–PA6–PTH, where PTH is poly(thionine)], with larger specific surface area and good biocompatibility used as supporting scaffolds for ssDNA1 immobilization, not only can dramatically increase the amount of DNA attachment and the hybridization sensitivity but also can have better stability. Through the hybridization reaction, a sandwich format of ssDNA1/K-ras gene/gold nanoparticle-labeled ssDNA2 (AuNPs–ssDNA2) was fabricated. The AuNPs–ssDNA2 offered electrochemical signal transduction. An amplification strategy through the formation of the network-like thiocyanuric acid/gold nanoparticles (TA/AuNPs) was presented, and the detection sensitivity improved noticeably. Finally, the detection limit of the K-ras gene biosensor and the discrimination between the K-ras gene and the one-base mismatched sequence were improved to some extent compared with the p53 biosensor. The experimental protocol is illustrated in Fig. 1. In this study, the characteristics of the sensing system for the detection of K-ras gene mutations and the analytical performance were examined. The amenability of this method to the analyses of K-ras from the SW480 colorectal cancer cell lysates was demonstrated.

Materials and methods

Reagents and apparatus

The DNA oligonucleotides in this study were obtained from Sangon Biotechnology (China). The oligonucleotide sequences are

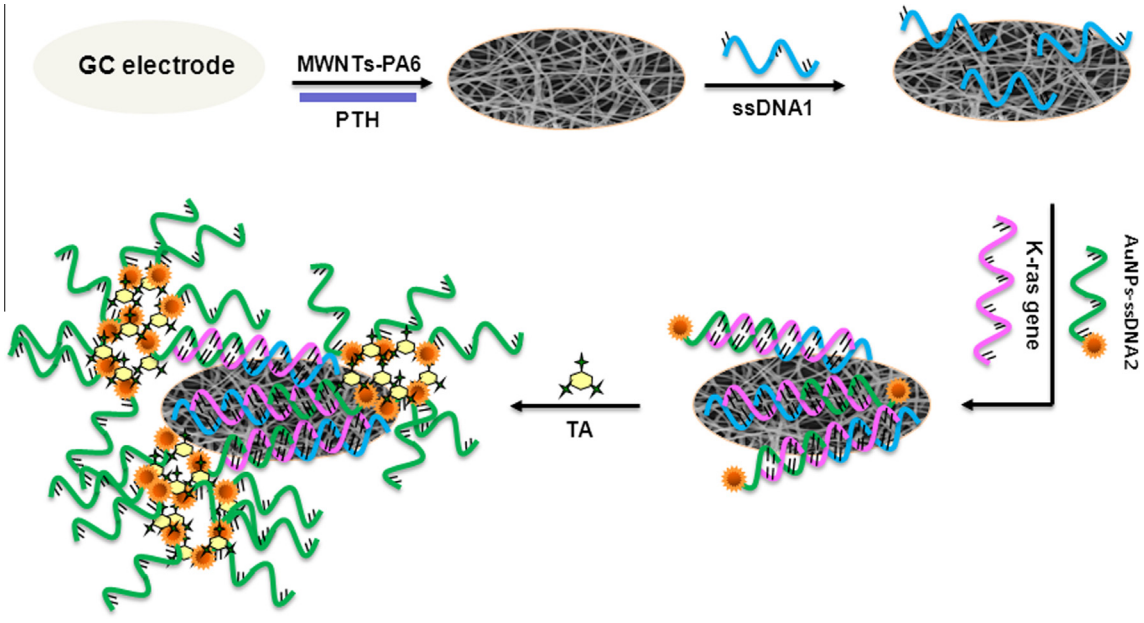

Fig.1. Schematic representation of the preparation of the electrochemical biosensor.

shown in Table 1. Thionine chloride, $HAuCl_4$, and thiocyanuric acid were purchased from Sigma (USA). Nylon 6 was purchased from Debiochem (China). SW480 colorectal cancer cells were purchased from Shanghai Institute of Life Science Cell Resource Center (China). A K-ras Kit (HRM: high-resolution melt) was purchased from HelixGen (China). Carboxylated multiwalled carbon nanotubes were obtained from Shenzhen Nanotech Port (China). The diameter was 40 to 60 nm, and the length was 1 to 10 μm. Other reagents were of analytical reagent grade. All of the solutions were prepared with ultrapure water from a Millipore Milli-Q system.

The field-emission scanning electron microscopy (FESEM) images were recorded using an S-4800 FE-SEM microscope (JEOL., Japan). A CHI 660D electrochemical analyzer (CHI Instruments, Chenhua, China) was used to carry out differential pulse voltammetry (DPV) and cyclic voltammetry (CV). A three-electrode system was used with the modified glassy carbon (GC) electrode (3 mm in diameter) as the working electrode, an Ag/AgCl (saturated) as the reference electrode, and a platinum wire as the counter electrode.

Preparation of modified electrodes

The surface of GC electrode was carefully polished with 0.3 μm Al_2O_3 powders successively, rinsed with water and ethanol in an ultrasonic bath briefly, and then allowed to dry at room temperature. PA6 and MWCNTs (0.1% of PA6) were dissolved in a mixture of cresol and formic acid (6:4, v/v) to obtain a homogeneous solution under vigorous stirring at room temperature. Electrospinning was carried out with a 20-ml syringe (1.2 mm diameter spinneret) at an electrical potential of 17 kV over an 18-cm gap between the spinneret and the cleaned GC surface at a rate of 1.2 ml/h. The ambient temperature and relative humidity for electrospinning were kept at 25 °C and 40%, respectively. It took 4 min to deposit the nanofibrous mat on the surface of the electrode. The as-prepared electrode was marked as MWCNTs–PA6 electrode.

Two different PTH-modified electrodes were carried out by two steps as follows:

(a) *MWCNTs–PA6–PTH electrode:* (i) holding the MWCNTs–PA6 electrode at 1.5 V for 10 min in 0.1 M phosphate-buffered saline (PBS, pH 6.0) containing 100 μM TH and (ii) potential scans for 15 cycles at 50 mV/s between −0.4 and 1.2 V (vs. Ag/AgCl) in the solution. A modest stir was going on through the electropolymerization. The electrode was washed with 0.1 M PBS (pH 6.0) to remove the adsorbed TH monomer thoroughly. The as-prepared electrode was denoted as MWCNTs–PA6–PTH electrode.

(b) *PTH electrode:* The PTH was modified on the bare GC electrode with the same processes as in (a). The as-prepared electrode was denoted as PTH electrode.

Preparation of AuNPs-labeled ssDNA2 probes

AuNPs with a diameter of 16 nm were prepared by citrate reduction of $HAuCl_4$ in aqueous solution according to the literature [35]. In brief, 100 ml of solution containing 0.01 g of $HAuCl_4$ was brought to reflux, and then 2.5 ml of 1% sodium citrate solution was introduced with stirring. The solution was kept boiling for 30 min and cooled to room temperature. The product was stored in a dark glass bottle at 4 °C for further use.

5′-Mercapto-capped ssDNA2 (the extinction coefficient was 178,200 L/(mol·cm), and the final concentration was 10 μM) in 10 mM PBS containing 0.8 M NaCl (pH 7.3) was mixed with 5 ml of the above fresh AuNPs solution for 40 h at 4 °C. The solution was followed by centrifugation at 14,000 rpm to remove excess ssDNA2. The red oily ssDNA2/AuNPs precipitate was washed with 10 mM PBS containing 0.8 M NaCl (pH 7.3) and redispersed in the above PBS. The AuNPs-labeled ssDNA2 probe was obtained. The concentrations of the AuNPs were determined using the absorbance values at 520 nm in conjunction with the molar absorption coefficient [36]. Approximately 25 to 30% of the original nanoparticle concentration was lost during centrifugation and workup. The concentration of the AuNPs-labeled ssDNA2 probe was calculated to be 8.6 μM according to the value of ultraviolet (UV) absorption of the ssDNA2 at 260 nm. The AuNPs–ssDNA2 probes were stored at 4 °C for later use.

Fabrication of electrochemical biosensing electrode

The MWCNTs–PA6–PTH electrode was immersed in 0.1 M acetic acid solution (pH 5.4) containing 1 μM ssDNA1, and a constant potential at +0.5 V (vs. Ag/AgCl) for 600 s was applied. Then the electrode was rinsed with 10 mM PBS (pH 7.3), and the ssDNA electrode was formed.

The ssDNA electrode was immersed in 10 mM PBS (pH 7.3, 0.8 M NaCl) containing K-ras sequence and AuNPs–ssDNA2 probes at 40 °C for 45 min. In this way, the double-stranded DNA (dsDNA) electrode was obtained. Then 10 μl of 10 μM TA was added into the above PBS. The dsDNA electrode was incubated in the PBS for 20 min at room temperature. The electrode was washed with 10 mM PBS (pH 7.3) to remove the unhybridized K-ras sequence, uncombined AuNPs–ssDNA2 probes, and the adsorbed dsDNA complex on the electrode surface thoroughly. The network-like

Table 1
Oligonucleotide sequences used in the experiment.

Description	Sequence
K-ras (associated with colorectal cancer)	
	5'-AAA***ACTTGTGGTAGTTGGAG***CTGA***TGGCGTAGGCAAGAGTGCCC***-3'
ssDNA1	3'-OH-$(CH_2)_6$-TTT***TGAACACCATCAACCTC***-$(CH_2)_6$-OH-5'
ssDNA2	3'-***ACCGCATCCGTTCTCACGGG***-$(CH_2)_6$-SH-5'
[a]**Mismach 1**	5'-AAAACTTGTG***C***TAGTTGGAGCTGATGGCGTAGGCAAGAGTGCCC-3'
[a]**Mismach 2**	5'-AAAACTTGTGGTAGTTGGAGCTGATGGCGTAGGC***T***AGAGTGCCC-3'

Note. The same color italic bases are complementary ones. (For interpretation of the reference to color in this table note, the reader is referred to the Web version of this article.)
[a]The underlined bases are mismatched ones.

TA/AuNPs dsDNA (TA/AuNPs–dsDNA) electrode was obtained and employed as working electrode to detect DPV signal.

Preparation of SW480 colorectal cancer cell lysates

The soluble cell lysates of the SW480 colorectal cancer cells were prepared according to Makmura and coworkers [37].The procedure is as follows. Cells were washed three times with ice-cold 10 mmol/L PBS containing 137 mmol/L NaCl and 2.7 mmol/L KCl (pH 7.4). After decanting the PBS solution, cells were lysed in 50 mmol/L Tris–HCl containing 150 mmol/L NaCl, 0.02% NaN_3, 0.1% sodium dodecyl sulfate (SDS), 100 μg/ml phenylmethanesulfonyl fluoride (PMSF), 1 μg/ml aprotinin, 1% Triton X-100, and 0.5% sodium deoxycholate (pH 8.0) on ice for 20 min. The lysed cells were then removed from the tube walls by a cell slicker and transferred to a centrifuge tube. After sonication for 30 s on ice, contents released from the cell were centrifuged at 4 °C at 12 000 rpm for 10 min. The supernatant was collected and stored at 4 °C for later use.

Measurement

DPV measurement 1

The DPV measurements were conducted by recording the reduction peak current at a potential of −0.14 V of the PTH-modified electrodes. The following parameters were used: pulse amplitude 0.05 V, pulse period 0.2 s, pulse width 0.05 s, and potential domain between −0.4 and 0.15 V (vs. Ag/AgCl). The electrolyte medium was 0.1 M PBS (pH 6.0).

DPV measurement 2

The electrochemical measurement signal of AuNPs was carried out by two steps: (i) the electrochemical oxidation of AuNPs of $AuCl_4^-$ was performed at 1.25 V for 120 s in 0.1 M HCl solution; (ii) immediately after the electrochemical oxidation, the DPV measurements were conducted from 0.8 to −0.1 V in the above HCl solution with a pulse amplitude of 0.05 V, a pulse width of 0.05 s, and pulse period of 0.2 s, resulting in a measurement signal due to the reduction of $AuCl_4^-$ that relates to the amount of the AuNPs for the sandwich format. The DPV peak height at a potential of 0.4 V of the reduction of $AuCl_4^-$ was used in all of the measurements.

Results and discussion

FESEM images of MWCNTs–PA6 composite nanofibers and MWCNTs–PA6–PTH electrode

The micro-morphologies of MWCNTs–PA6 composite nanofibers and MWCNTs–PA6–PTH electrode were analyzed using FESEM, as shown in Fig. 2. MWCNTs–PA6 composite nanofibers with smooth surface are evenly distributed on the substrate, and their orientations are random. The diameters of the nanofibers range from 60 to 300 nm (Fig. 2A). A three-dimensional (3D) porous and dense modification layer on the electrode surface was obtained for MWCNTs–PA6–PTH electrode (Fig. 2B). Quantitative estimation of the average pore diameter of the above nanofibers was performed. Compared with the MWCNTs–PA6 composite nanofibers, the average pore diameter of the MWCNTs–PA6–PTH electrode decreased from 0.39 to 0.24 μm. In this case, MWCNTs–PA6 composite nanofibers served as the nanosized backbone for TH polymerization, resulting in the porous PTH film covered around the MWCNTs–PA6 composite nanofibers in a cylinder structure. In this way, a significant increase of the PTH amount around MWCNTs–PA6 composite nanofibers was generated.

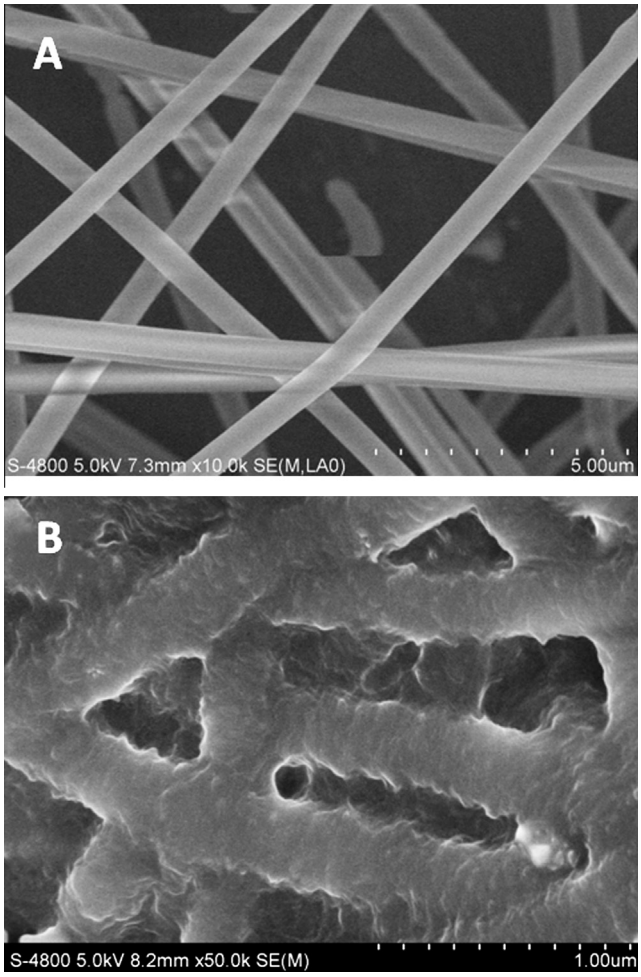

Fig.2. FESEM images of MWCNTs–PA6 composite nanofibers (A) and MWCNTs–PA6–PTH electrode (B).

Finally, the MWCNTs–PA6–PTH electrode with coarser nanofibers and a smaller pore diameter was obtained.

Characterization of PTH film

In this study, the PTH-modified electrodes were obtained by a simple two-step method. After a preanodization at 1.5 V for 10 min, the cyclic voltammograms were scanned between −0.4 and 1.2 V for the bare GC electrode and the MWCNTs–PA6 electrode (Fig. 3A). It indicated the growth process of the PTH film on electrode surface with consecutive cycles. During the process of TH electropolymerization onto electrode surface, the currents of a pair of reversible redox peaks continued to build up with every successive sweep, indicating an increase in quantity of electroactive species on the electrode. By removing the electrode from TH-containing solution, a golden and purple film was formed on the electrode surface. As shown in Fig. 3A, a marked increase in the CV peak currents for the MWCNTs–PA6 electrode (solid line) compared with the bare electrode (dash dot line) is observed. It is also seen that the electrochemical surface area of the MWCNTs–PA6 electrode was significantly increased in contrast to the bare electrode. As a result, the amounts of the PTH around MWCNTs–PA6 composite nanofibers were increased significantly. It can be attributed to a large surface area of each MWCNTs–PA6 composite nanofiber, which can be regarded as an independent microelectrode when the electropolymerization reaction takes

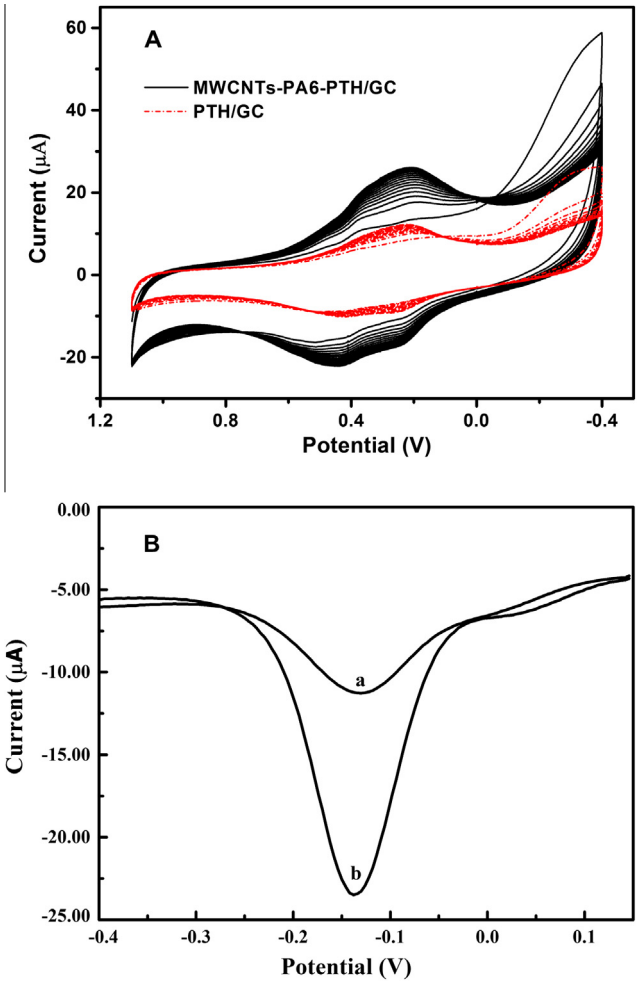

Fig.3. (A) Repetitive CV curves for the electropolymerization of TH onto MWCNTs–PA6 (solid line) and bare GC electrode (dash dot line) surface in 0.1 M PBS (pH 6.0) containing 100 μM TH with 15 continuous cyclic scans between −0.4 and 1.2 V (vs. Ag/AgCl) at 50 mV/s. Before the electropolymerization, the electrode went on a preanodization at 1.5 V in the TH solution for 10 min. (B) DPV responses for the PTH electrode (curve a) and the MWCNTs–PA6–PTH (curve b) scanning from −0.40 to 0.15 V in 0.1 M PBS (pH 6.0).

place on the MWCNTs–PA6 electrode. Finally, the MWCNTs–PA6–PTH electrode with a larger electrochemical surface area was obtained.

The PTH film was electroactive because each monomer unit retained its electroactive heterocyclic nitrogen atom. Moreover, as polymerization occurred, a large amount of positive charges was accumulated on the electrode surface and used to create the TH cation radicals. These active cation radicals were linked through the –NH– bridge to form PTH film with a 3D porous structure onto electrode surface. Those bridges between monomer units, as in polyaniline films, were electroactive [38]. The preanodization operation was critical. If the CV scans were directly carried out without an oxidation pretreatment or with a preanodization potential lower than 1.1 V, there was not enough positive charges accumulated on electrode to create TH cation radicals, which resulted in a failing electropolymerization of TH because there was no current growth under the same polymerization conditions. However, if the preanodization was conducted below 1.5 V, the polymer film was not strongly attached to the electrode and destroyed by wash in PBS with stirring. Hence, in the current experiment, 1.5 V was used as the pretreatment potential. The pH value of the electropolymerization solution had a significant effect on the electropolymerization process of the PTH. During the near neutral biocompatible pH range (pH 6.0–8.0), pH 6.0 resulted in the best reversible and conductive PTH film onto electrode surface. Therefore, pH 6.0 was chosen as the pH value of the electropolymerization solution in this work. This result was in accordance with Ref. [39]. As shown in Fig. 3B, there was a marked increase in the DPV peak currents for the MWCNTs–PA6–PTH electrode compared with the PTH electrode with scanning between −0.4 and 0.15 V (vs. Ag/AgCl) as in DPV measurement 1. Besides, the MWCNTs–PA6–PTH electrode was stable in 0.1 M PBS (pH 6.0) without change of the PTH redox peak current after 2 days. This property made MWCNTs–PA6–PTH electrode suitable to sensitively detect DNA hybridization under biocompatible conditions.

CV behavior of different modified electrodes

The fabrication processes of the electrochemical biosensor were characterized by CV using $[Fe(CN)_6]^{3-/4-}$, as shown in Fig. 4. A symmetric and reversible voltammogram was obtained for a bare GC electrode (curve b). Compared with the former one, the voltammogram observed at the MWCNTs–PA6 electrode (curve c) displayed a slight decline in the redox current. It is consistent with the fact that a trace amount of MWCNTs had no effect on the conductivity of the PA6, but MWCNTs could increase the mechanical stability of nanofibers and make them more durable under operating conditions [40,41]. A significant increase was presented in the redox current for MWCNTs–PA6–PTH electrode (curve a). In this case, the TH polymerization was taking place on the MWCNTs–PA6 composite nanofibers that served as the nanosized backbone. A positive charged PTH film with a 3D porous structure was formed around the MWCNTs–PA6 composite nanofibers. The outstanding charge transport characteristics of the positive charged PTH film and the electrostatic attractive force to $[Fe(CN)_6]^{3-/4-}$ led to the increase in the redox current. Once the ssDNA1 was adsorbed onto the MWCNTs–PA6–PTH electrode by electrostatic interactions, asymmetric and irreversible waves accompanied by a decline in the redox current were obtained for the ssDNA electrode (curve d). This resulted in the ssDNA1, which has a single-strand nucleic acid with negative charges on its phosphate backbone, making an electrostatic repulsive force to $[Fe(CN)_6]^{3-/4-}$. When the dsDNA electrode was formed, the increase in the amount of nucleic acid

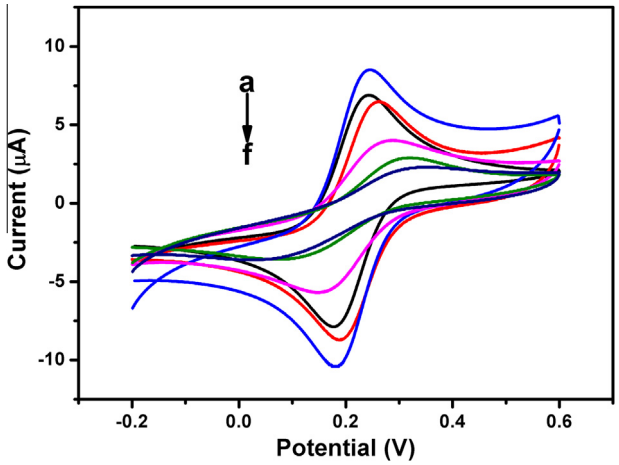

Fig.4. CV curves in 1 mM $[Fe(CN)_6]^{3-/4-}$ solution for the MWCNTs–PA6–PTH electrode (a), bare GC electrode (b), MWCNTs–PA6 electrode (c), ssDNA electrode (d), dsDNA electrode (e), and TA/AuNPs–dsDNA electrode (f). The signal amplification was implemented in 10 mM PBS (pH 7.3) and 0.8 M NaCl (after hybridization) containing 10 μl of 10 μM TA for 20 min at room temperature. Scan rate: 0.1 V/s; scan range: −0.2 to 0.6 V.

made a stronger repulsive force to $[Fe(CN)_6]^{3-/4-}$. As a result, a further decrease was presented in the redox current for the dsDNA electrode (curve e). The signal amplification was further implemented by forming network-like TA/AuNPs, and a large number of AuNPs–ssDNA2 probes accumulated on the surface of the electrode. Therefore, a further decline was found in the redox current for the TA/AuNPs–dsDNA electrode (curve f). The change in the CV curves of the electrodes illustrated the successful modification of the biosensing components onto the GC electrode. It also indicated that the interactions between the MWCNTs–PA6–PTH and the ssDNA1, as well as the K-ras gene and the two complementary ssDNA electrodes, had occurred.

Characterization of electrochemical biosensor

Here, three different design concepts of the electrochemical biosensor for detection of the K-ras gene were investigated. The PTH electrode (the TH electropolymerization process for the PTH electrode was the same as that for the MWCNTs–PA6–PTH electrode, and the concentration of TH was also the same) was used to fabricate the sandwich format of ssDNA1/K-ras gene/AuNPs–ssDNA2 without adding TA (Fig. 5, curve a) or with adding TA for signal amplification (Fig. 5, curve b), and the MWCNTs–PA6–PTH electrode was used to prepare the sandwich format of ssDNA1/K-ras gene/AuNPs–ssDNA2 with adding TA for signal amplification (Fig. 5, curve c). As shown in curve a of Fig. 5, the DPV peak current (I_p) of the AuNPs at 0.4 V (vs. Ag/AgCl) is very small (design concept a). In contrast, with signal amplification by adding TA (design concept b), the I_p is approximately 4 times higher compared with the former one (Fig. 5, curve b). In other words, a significant sensitivity enhancement was obtained with the signal amplification. This owes to the fact that TA can easily cap more AuNPs to form network-like TA/AuNPs by the strong interaction among AuNPs and three thiol groups of each TA molecule. As shown in curve c of Fig. 5, using the MWCNTs–PA6–PTH electrode and signal amplification by adding TA (design concept c), the I_p was magnified 2 times compared with design concept b. It is consistent with the fact that the functional composite nanofibers (MWCNTs–PA6–PTH) with large specific surface area and good biocompatibility used as supporting scaffolds for ssDNA immobilization can dramatically increase the amount of DNA attachment and the

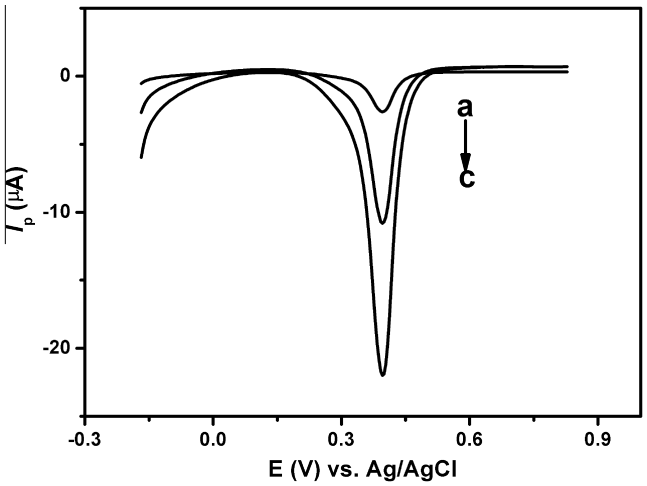

Fig.5. DPV responses for various dsDNA electrodes. The PTH electrode was used to fabricate of the sandwich format without (a) or with (b) signal amplification, and the MWCNTs–PA6–PTH electrode was used to prepare the sandwich format with signal amplification (c). The electrochemical measurement signal of AuNPs was carried out by two steps in 0.1 M HCl solution. The concentration of the K-ras gene was 10 pM.

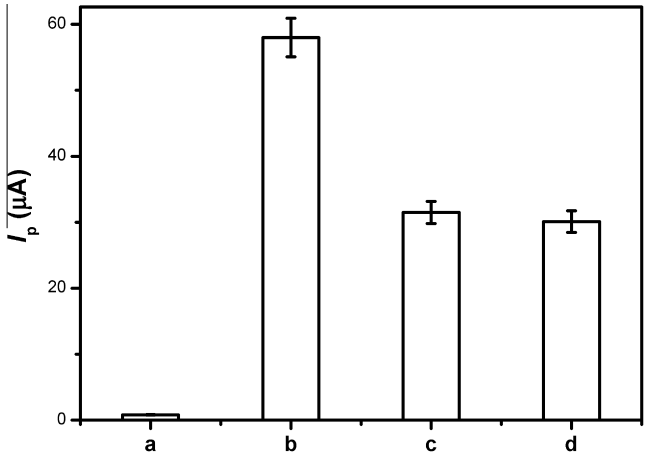

Fig.6. DPV responses for various TA/AuNPs–dsDNA electrodes: (a) blank; (b) 10 nM K-ras; (c) 10 nM one-base mismatched sequence of the K-ras (G/C mismatched); (d) 10 nM one-base mismatched sequence of the K-ras (A/T mismatched). The electrochemical measurement signal of AuNPs was carried out by two steps.

hybridization sensitivity. It is worth mentioning that the I_p from design concept c was cumulatively magnified 8 times compared with design concept a. The above results proved that our design concept of the electrochemical biosensor for detection of the K-ras gene is feasible and can bring ultrasensitivity for the target detection.

The binding specificity of the ssDNA electrode was investigated by the control hybridization experiments for K-ras (complementary sequence of the ssDNA1), one-base mismatched sequence of the K-ras (G/C mismatched), one-base mismatched sequence of the K-ras (A/T mismatched), and the blank. As shown in column a of Fig. 6, the I_p values of the AuNPs at 0.4 V (vs. Ag/AgCl) are almost negligible after the process of hybridization with the blank. However, the largest I_p was detected when the ssDNA electrode was hybridized with K-ras (Fig. 6, column b). Meanwhile, the one-base mismatched DNA (G/C mismatched) (Fig. 6, column c) and the one-base mismatched DNA (A/T mismatched) (Fig. 6, column d) turn out to be approximately 54.3 and 51.9% signal from the K-ras when they are in the same concentration. In other words, the discriminations of the K-ras and G/C mismatched DNA and of the K-ras and A/T mismatched DNA are 54.3 and 51.9% using the MWCNTs–PA6–PTH electrodes, respectively. The consistent data were obtained when the experiment was repeated three times. The results show that the MWCNTs–PA6–PTH-based DNA hybridization assay has high selectivity from the one-base mismatched sequence. The relative standard deviation (RSD) of the I_p for the six repeated detections of K-ras (10 nM) was 4.87%, indicating the good reproducibility of this method. The stability of the ssDNA electrode was investigated on 5, 8, 10, 12, and 15 days storage at 4 °C and further used to hybridize with the target K-ras sequence; fully 97.4% of the initial sensitivity remained after 10 days, indicating that this modified electrode was a stable platform as an electrochemical DNA biosensor. In summary, the electrochemical biosensor demonstrated good performance, including higher binding specificity, long shelf life, and excellent reproducibility.

Optimization of experimental conditions

To maximize the detection sensitivity of the proposed electrochemical biosensor, various conditions were optimized by single factor experiments. In 4 min, the MWCNTs–PA6 nanofibrous mat was deposited on the surface of the GC electrode and was visible directly. The cycles of CV for TH electropolymerization were inves-

tigated. As shown in Fig. 3A, with the increase of the scan cycle number, scanning current gradually increased and increased slowly after 15 cycles. For conventional studies, the performance of conducting polymer is strongly influenced by the thickness of the polymer film. Increasing the film thickness will deteriorate the hybridization detection sensitivity [42]. In consideration of the analysis time and sensitivity, we employed 15 cycles of CV in a range of −0.4 to 1.2 V for TH electropolymerization with a scan rate of 50 mV/s.

The efficiency of the hybridization is in correlation with the ionic strength of the hybridization buffer, hybridization time, and hybridization temperature. The I_p of the AuNPs at 0.4 V (vs. Ag/AgCl) decreased with the increasing NaCl concentration and hybridization time. It reached plateau regions at the NaCl concentration of 0.8 M and the hybridization time of 45 min. Thus, the optimal NaCl concentration and hybridization time were chosen at 0.8 M and 45 min, respectively. The curve of the I_p varied with the hybridization temperature from 10 to 60 °C, with 10 °C increments, and was like a parabola with its peak at 40 °C. So, 40 °C was chosen as the optimal hybridization temperature.

AuNPs have good electrochemical response in acid medium. The strongest I_p of the AuNPs was detected in the HCl detecting solution when the H_2SO_4 and HNO_3 detecting solutions were in the same concentration. It resulted in the gold ion (Au^{3+}) and Cl^- being able to generate stable $AuCl_4^-$. The concentration of the HCl detecting solution was selected according to the literature [40]. So, 0.1 M HCl solution was selected as the DPV detecting solution.

Calibration curve of K-ras detection

The sensitivity of the electrochemical biosensor was investigated. The DPV responses for various TA/AuNPs–dsDNA electrodes are shown in Fig. 7. The peak current difference [ΔI_p, where $\Delta I_p = I_p(\text{K-ras}) - I_p(\text{blank})$] of AuNPs reduction grew when the K-ras concentration increased, and the ΔI_p was linear to the logarithm of K-ras concentration ranging from 0.1 to 100 pM (as shown in the Fig. 7 inset). The equation for the resulting calibration plot was $y = 8.14\lg x + 4.24$ (where x was the concentration of K-ras and y was the ΔI_p), with correlation coefficient as 0.9991. The detection limit for K-ras of 30 fM was estimated using 3σ (where σ is the relative standard deviation of a blank solution, $n = 11$).

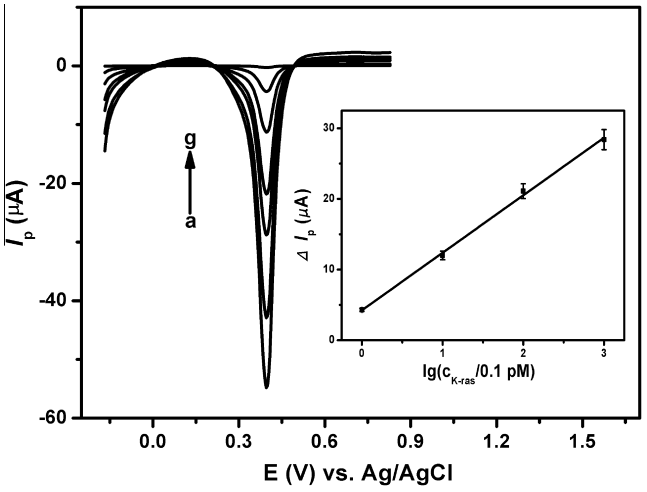

Fig.7. DPV responses for various TA/AuNPs–dsDNA electrodes. The concentrations of K-ras were 10 nM (a), 1 nM (b), 100 pM (c), 10 pM (d), 1 pM (e), 0.1 pM (f), and 0 M (g). Inset: Related calibration plot versus K-ras concentrations in a range from 0.1 to 100 pM.

Table 2
Test results of soluble cell lysates of SW480 colorectal cancer cells.

Cell lysates	K-ras (this method) (pM)	K-ras Kit (HRM) (pM)
SW480 colorectal cancer cells	7.9	8.7

The consistent data were obtained as shown in the error bars in the Fig. 7 inset when the experiment was repeated three times.

Analysis of SW480 colorectal cancer cell lysates

Finally, the amenability of this method to analyses of the K-ras gene from SW480 colorectal cancer cell lysates was demonstrated. Through the hybridization reaction, a sandwich format of ssDNA1/K-ras gene (the soluble cell lysates of the SW480 colorectal cancer cells)/AuNPs–ssDNA2 was fabricated. The signal amplification was further implemented by the formation of the network-like TA/AuNPs. The DPV peak height at 0.4 V was detected. To further validate the method for clinical applications, HRM (K-ras Kit) tests were compared with the developed method for the analyses of the soluble cell lysates of the SW480 colorectal cancer cells. First, the K-ras gene fragments in the soluble cell lysates of the SW480 colorectal cancer cells were specifically amplified by PCR. Then, HRM was designed to monitor fluorescence change and produced a melting profile. As shown in Table 2, the results of the electrochemical biosensor are basically consistent with those of the K-ras Kit (HRM). The consistent data were obtained when the experiment was repeated three times. The method was capable of determining K-ras from real samples without extensive sample pretreatment/separation or specialized instruments. It holds promise as a clinical protocol for assaying K-ras DNA binding capacity in normal and cancer cells at sensitive levels.

Conclusions

An electrochemical biosensor based on functional composite nanofibers for hybridization detection of a specific mutation in the K-ras gene has been developed. The MWCNTs–PA6–PTH electrode with unique 3D nanostructure, large specific surface area, and good biocompatibility was proposed and can be used to enhance stability, speed, and sensitivity. Through the hybridization reaction, a sandwich format of ssDNA1/K-ras gene/AuNPs–ssDNA2 was fabricated, and the signal amplification was further implemented by forming network-like TA/AuNPs. A significant sensitivity enhancement was obtained; the detection limit was down to 30 fM, and the discriminations were up to 54.3 and 51.9% between the K-ras gene and the one-base mismatched sequences including G/C and A/T mismatched bases, respectively. The sensor system was successfully applied to analyze K-ras from the SW480 colorectal cancer cell lysates. The results of the electrochemical biosensor are basically consistent with those of the K-ras Kit (HRM). The proposed biosensor has been demonstrated to offer a convenient, specific, and sensitive method of detecting gene mutation. Moreover, the nanofibers modified electrode and the amplification strategy are expected to have wide applications in other biomolecule monitoring and disease diagnosis.

Acknowledgments

This project was supported by the National Nature Science Foundation of China (81302472, 81172721, and 81172697), the Doctoral Program of Higher Education of China (20110092 120055), and the Students' Innovation Experimental Project of China (S2014118).

References

[1] B. Vogelstein, K.W. Kinzler, Cancer genes and the pathways they control, Nat. Med. 10 (2004) 789–799.
[2] K. Wennerberg, K.L. Rossman, C.J. Der, The Ras superfamily at a glance, J. Chem. Soc. 118 (2005) 843–846.
[3] S. Velho, K.M. Haigis, Regulation of homeostasis and oncogenesis in the intestinal epithelium by Ras, Exp. Cell Res. 317 (2011) 2732–2739.
[4] N. Charette, C. Vandeputte, P. Starkel, Ras in digestive oncology: from molecular biology to clinical implications, Curr. Opin. Oncol. 26 (2014) 454–461.
[5] T.K. Er, C.C. Chen, L. Bujanda, M. Herreros-Villanueva, Clinical relevance of KRAS mutations in codon 13: where are we?, Cancer Lett 343 (2014) 1–5.
[6] Y. Pylayeva-Gupta, E. Grabocka, D. Bar-Sagi, RAS oncogenes: weaving a tumorigenic web, Nat. Rev. Cancer 11 (2011) 761–774.
[7] A.E. Karnoub, R.A. Weinberg, Ras oncogenes: split personalities, Nat. Rev. Mol. Cell Biol. 9 (2008) 517–531.
[8] Y.X. Wang, C.E. Kaiser, B. Frett, H.Y. Li, Targeting mutant KRAS for anticancer therapeutics: a review of novel small molecule modulators, J. Med. Chem. 56 (2013) 5219–5230.
[9] J. Chen, M.V. Viola, A method to detect ras point mutations in small subpopulations of cells, Anal. Biochem. 195 (1991) 51–56.
[10] C.P. Dieterle, M. Conzelmann, U. Linnemann, M.R. Berger, Detection of isolated tumor cells by polymerase chain reaction–restriction fragment length polymorphism for K-ras mutations in tissue samples of 199 colorectal cancer patients, Clin. Cancer Res. 10 (2004) 641–650.
[11] M. Imai, T. Hoshi, K. Ogawa, K-RAS codon-12 mutations in biliary tract tumors detected by polymerase chain reaction denaturing gradient gel electrophoresis, Cancer 73 (1994) 2727–2733.
[12] P. Malhotra, M. Anwar, N. Nanda, R. Kochhar, J.D. Wig, K. Vaiphei, S. Mahmood, Alterations in K-ras, APC, and p53 multiple genetic pathway in colorectal cancer among Indians, Tumor Biol. 34 (2013) 1901–1911.
[13] D. Calistri, C. Rengucci, I. Seymour, A. Lattuneddu, A.M. Polifemo, F. Monti, L. Saragoni, D. Amadori, Mutation analysis of p53, k-ras, and BRAF genes in colorectal cancer progression, J. Cell. Physiol. 204 (2005) 484–488.
[14] J.H. Park, S.W. Han, D.Y. Oh, S.A. Im, S.Y. Jeong, K.J. Park, T.Y. Kim, Y.J. Bang, J.G. Park, Analysis of KRAS, BRAF, PTEN, IGF1R, EGFR intron 1 CA status in both primary tumors and paired metastases in determining benefit from cetuximab therapy in colon cancer, Cancer Chemother. Pharmacol. 68 (2011) 1045–1055.
[15] A. Jarry, D. Masson, E. Cassagnau, S. Parois, C. Laboisse, M.G. Denis, Real-time allele-specific amplification for sensitive detection of the BRAF mutation V600E, Mol. Cell. Probes 18 (2004) 349–352.
[16] A.H. Lang, H. Drexel, S. Geller-Rhomberg, N. Stark, T. Winder, K. Geiger, A. Muendlein, Optimized allele-specific real-time PCR assays for the detection of common mutations in KRAS and BRAF, J. Mol. Diagn. 13 (2011) 23–28.
[17] K. Balschun, A.K. Wenke, C. Röcken, J. Haag, Detection of KRAS and BRAF mutations in advanced colorectal cancer by allele-specific single-base primer extension, Expert Rev. Mol. Diagn. 11 (2011) 799–802.
[18] S. Magnin, E. Viel, A. Baraquin, S. Valmary-Degano, B. Kantelip, J.L. Pretet, C. Mougin, M. Bigand, B. Girardo, C. Borg, C. Ferrand, A multiplex sNaPshot assay as a rapid method for detecting KRAS and BRAF mutations in advanced colorectal cancers, J. Mol. Diagn. 13 (2011) 485–492.
[19] L.Q. Lin, A.L. Liu, C.F. Zhao, S.H. Weng, Y. Lei, Q.C. Liu, X.H. Lin, Y.Z. Chen, A chronocoulometric LNA sensor for amplified detection of K-ras mutation based on site-specific DNA cleavage of restriction endonuclease, Biosens. Bioelectron. 42 (2013) 409–414.
[20] L.Q. Lin, S.H. Weng, C.F. Zhao, Q.C. Liu, A.L. Liu, X.H. Lin, Hairpin LNA biosensor with enzyme tagged AuNPs as tracer for amperometric detection of K-ras mutation gene, Electrochim. Acta 108 (2013) 808–813.
[21] Z.J. Wang, Y.H. Yang, K.L. Leng, J.S. Li, F. Zheng, G.L. Shen, R.Q. Yu, A sequence-selective electrochemical DNA biosensor based on HRP-labeled probe for colorectal cancer DNA detection, Anal. Lett. 41 (2008) 24–35.
[22] Y. Kam, A. Rubinstein, A. Nissan, D. Halle, E. Yavin, Detection of endogenous K-ras mRNA in living cells at a single base resolution by a PNA molecular beacon, Mol. Pharm. 9 (2012) 685–693.
[23] A. Okumura, Y. Sato, M. Kyo, H. Kawaguchi, Point mutation detection with the sandwich method employing hydrogel nanospheres by the surface plasmon resonance imaging technique, Anal. Biochem. 339 (2005) 328–337.
[24] B.L. Xing, J.Z. Song, S.M. Ge, Z.H. Tang, M.L. Liu, Q. Yang, F.T. Lü, L.B. Liu, S.C. Wang, Multiplex detection of KRAS and BRAF mutations using cationic conjugated polymers, Chin. Sci. Bull. 58 (2013) 873–878.
[25] D.B. Zhu, D. Xing, Y.B. Tang, X.M. Zhou, Detection of K-ras point mutation in pancreatic cancer by electrochemiluminescence–polymerase chain reaction, Chin. J. Anal. Chem. 35 (2007) 751–753.
[26] D.B. Zhu, D. Xing, Y.B. Tang, L. Zhang, A novel mutant allele specific amplification and electrochemiluminescence method for the detection of point mutation in clinical samples, Biosens. Bioelectron. 24 (2009) 3306–3310.
[27] Z.H. Dai, H.X. Ju, Bioanalysis based on nanoporous materials, Trends Anal. Chem. 39 (2012) 149–162.
[28] A.L. Liu, K. Wang, S.H. Weng, Y. Lei, L.Q. Lin, W. Chen, X.H. Lin, Y.Z. Chen, Development of electrochemical DNA biosensors, Trends Anal. Chem. 37 (2012) 101–111.
[29] S.H. Jiang, H.Q. Hou, A. Greiner, S. Agarwal, Tough and transparent nylon-6 electrospun nanofiber reinforced melamine–formaldehyde composites, Appl. Mater. Interfaces 4 (2012) 2597–2603.
[30] Z.G. Wang, L.S. Wan, Z.M. Liu, X.J. Huang, Z.K. Xu, Enzyme immobilization on electrospun polymer nanofibers: an overview, J. Mol. Catal. B 56 (2009) 189–195.
[31] S. Marx, M.V. Jose, J.D. Andersen, A.J. Russell, Electrospun gold nanofiber electrodes for biosensors, Biosens. Bioelectron. 26 (2011) 2981–2986.
[32] P. Ekabutr, O. Chailapakul, P. Supaphol, Modification of disposable screen-printed carbon electrode surfaces with conductive electrospun nanofibers for biosensor applications, J. Appl. Polym. Sci. 130 (2013) 3885–3893.
[33] S.J. Lee, R. Tatavarty, M.B. Gu, Electrospun polystyrene–poly(styrene-co-maleic anhydride) nanofiber as a new aptasensor platform, Biosens. Bioelectron. 38 (2012) 302–307.
[34] X.Y. Wang, X.B. Wang, X.N. Wang, F.T. Chen, K.H. Zhu, Q. Xu, M. Tang, Novel electrochemical biosensor based on functional composite nanofibers for sensitive detection of p53 tumor suppressor gene, Anal. Chim. Acta 765 (2013) 63–69.
[35] A. Doron, E. Katz, I. Willner, Organization of Au colloids as monolayer films onto ITO glass surfaces: application of the metal colloid films as base interfaces to construct redox-active monolayers, Langmuir 11 (1995) 1313–1317.
[36] L.M. Demers, C.A. Mirkin, R.C. Mucic, R.A. Reynolds III, R.L. Letsinger, R. Elghanian, G. Viswanadham, A fluorescence-based method for determining the surface coverage and hybridization efficiency of thiol-capped oligonucleotides bound to gold thin films and nanoparticles, Anal. Chem. 72 (2000) 5535–5541.
[37] L. Makmura, M. Hamann, A. Areopagita, S. Furuta, A. Muñoz, J. Momand, Development of a sensitive assay to detect reversibly oxidized protein cysteine sulfhydryl groups, Antioxid. Redox Signal. 3 (2001) 1105–1118.
[38] J.M. Bauldreay, M.D. Archer, Dye-modified electrodes for photogalvanic cells, Electrochim. Acta 28 (1983) 1515–1522.
[39] Y. Xu, Y. Jiang, L. Yang, P.G. He, Y.Z. Fang, Direct electrochemical detection of oligonucleotide hybridization on poly(thionine) film, Chin. J. Chem. 23 (2005) 1665–1670.
[40] Y. Dror, W. Salalha, R.L. Khalfin, Y. Cohen, A.L. Yarin, E. Zussman, Carbon nanotubes embedded in oriented polymer nanofibers by electrospinning, Langmuir 19 (2003) 7012–7020.
[41] J.S. Jeong, S.Y. Jeon, T.Y. Lee, J.H. Park, J.H. Shin, P.S. Alegaonkar, A.S. Berdinsky, J.B. Yoo, Fabrication of MWNTs/nylon conductive composite nanofibers by electrospinning, Diamond Relat. Mater. 15 (2006) 1839–1843.
[42] H. Cai, Y. Xu, P.G. He, Y.Z. Fang, Indicator free DNA hybridization detection by impedance measurement based on the DNA-doped conducting polymer film formed on the carbon nanotube modified electrode, Electroanalysis 15 (2003) 23–24.